European Radiology

MAGNETIC RESONANCE

Assessment of pulmonary physiological changes caused by aging, cigarette smoking, and COPD with hyperpolarized ^{129}Xe magnetic resonance

Qiuchen Rao[1], Haidong Li[1,2], Qian Zhou[1], Ming Zhang[1,2], Xiuchao Zhao[1,2], Lei Shi[1,2], Junshuai Xie[1,2], Li Fan[3], Yeqing Han[1,2], Fumin Guo[1], Shiyuan Liu[3] and Xin Zhou[1,2,4*]

Abstract

Objective To comprehensively assess the impact of aging, cigarette smoking, and chronic obstructive pulmonary disease (COPD) on pulmonary physiology using ^{129}Xe MR.

Methods A total of 90 subjects were categorized into four groups, including healthy young (HY, $n = 20$), age-matched control (AMC, $n = 20$), asymptomatic smokers (AS, $n = 28$), and COPD patients ($n = 22$). ^{129}Xe MR was utilized to obtain pulmonary physiological parameters, including ventilation defect percent (VDP), alveolar sleeve depth (h), apparent diffusion coefficient (ADC), total septal wall thickness (d), and ratio of xenon signal from red blood cells and interstitial tissue/plasma (RBC/TP).

Results Significant differences were found in the measured VDP ($p = 0.035$), h ($p = 0.003$), and RBC/TP ($p = 0.003$) between the HY and AMC groups. Compared with the AMC group, higher VDP ($p = 0.020$) and d ($p = 0.048$) were found in the AS group; higher VDP ($p < 0.001$), d ($p < 0.001$) and ADC ($p < 0.001$), and lower h ($p < 0.001$) and RBC/TP ($p < 0.001$) were found in the COPD group. Moreover, significant differences were also found in the measured VDP ($p < 0.001$), h ($p < 0.001$), ADC ($p < 0.001$), d ($p = 0.008$), and RBC/TP ($p = 0.032$) between the AS and COPD groups.

Conclusion Our findings indicate that pulmonary structure and functional changes caused by aging, cigarette smoking, and COPD are various, and show a progressive deterioration with the accumulation of these risk factors, including cigarette smoking and COPD.

Clinical relevance statement Pathophysiological changes can be difficult to comprehensively understand due to limitations in common techniques and multifactorial etiologies. ^{129}Xe MRI can demonstrate structural and functional changes caused by several common factors and can be used to better understand patients' underlying pathology.

Key Points

- *Standard techniques for assessing pathophysiological lung function changes, spirometry, and chest CT come with limitations.*
- *^{129}Xe MR demonstrated progressive deterioration with accumulation of the investigated risk factors, without these limitations.*
- *^{129}Xe MR can assess lung changes related to these risk factors to stage and evaluate the etiology of the disease.*

Qiuchen Rao, Haidong Li, and Qian Zhou contributed equally to this work.

*Correspondence:
Xin Zhou
xinzhou@wipm.ac.cn
Full list of author information is available at the end of the article

Springer

Keywords Magnetic resonance, Aging, Cigarette smoking, Chronic obstructive pulmonary disease, Lung

Introduction

Chronic obstructive pulmonary disease (COPD) is the third leading cause of death globally. More than 200 million COPD cases were reported globally, including more than 3.2 million deaths in 2019 [1]. Cigarette smoking is the most important cause of COPD, and most COPD patients have a history of smoking [2]. In addition, COPD is inherently associated with aging [2], and the prevalence is much higher among the elderly. Many features in the aging lung are similar to that in the lung of COPD patients, including a decline in lung function, increased gas trapping, loss of lung elastic recoil and parenchymal tissue, and enlargement of distal air spaces [3]. Notably, cellular damage resulting from both aging and cigarette smoking might involve interrelated pathogenetic mechanisms, as aging may lower the injury threshold or amplify the mechanisms involved in lung destruction by cigarette smoke [4]. A better understanding of how these risk factors affect the pulmonary physiological changes may facilitate the identification of the causes of lung injury and the development of novel and effective lung disease treatments.

Spirometry is currently used for the diagnosis of COPD and evaluation of treatment efficacy. The established cutoff for COPD diagnosis is an FEV_1/FVC ratio of less than 0.7 [5]. Nevertheless, spirometry measurements may be influenced by patient compliance and biased by age, resulting in overdiagnosis of COPD among the elderly and underdiagnosis in young adults [6]. In addition, spirometry could only assess the global information of lung function while it is widely recognized that lung disease is spatially heterogeneous. Computed tomography (CT) is widely used for the diagnosis of COPD, particularly in the assessment of emphysema and bronchiolar inflammation in clinic [7]. Nonetheless, chest CT involves substantial ionizing radiation and could hardly assess pulmonary gas-transfer function, which is the fundamental physiological function of the lung [8].

Hyperpolarized (HP) ^{129}Xe magnetic resonance (MR) has been regarded as a promising imaging modality for regional and sensitive pulmonary structure and function assessment without the limitations of spirometry and chest CT. This technique enables non-invasive evaluations of pulmonary ventilation, terminal airway morphology, and gas-transfer function [9], and has been employed to assess lung injuries caused by cigarette smoking and COPD [10–13]. ^{129}Xe ventilation imaging has been used to quantify the impaired pulmonary function in patients with COPD and other diseases [10, 14], and ventilation heterogeneity has been observed in healthy elderly never-smokers [15], ex-smokers without airflow limitation [16], and asymptomatic smokers [17]. Additionally, pulmonary morphological parameters provided by diffusion-weighted ^{129}Xe MRI have demonstrated potential for early detection of pulmonary microstructural changes associated with emphysema [11, 18, 19]. Moreover, ^{129}Xe MR has also been utilized to evaluate the gas-transfer function changes caused by COPD and smoking and greater septal wall thickness was found in subjects with COPD [20–22].

HP gas MR has also been used for assessing the impact of aging on the pulmonary physiology. Quirk and colleagues investigated the relationships between the morphometric parameters of lung acinar airways and aging [23]. Other studies showed that age could affect the gas-transfer function of the lung in children and adults [24]. Our previous work also explored the relationships between pulmonary physiological parameters and aging in a relatively small population [20]. Of note, previous noble gas MR studies of aging typically assessed morphometric parameters or gas-transfer function separately, and a comprehensive assessment of the influence of aging on lung structural and functional parameter changes is lacking. In addition, it is challenging to isolate the influence of aging when assessing the physiological changes resulting from cigarette smoking or COPD.

Collectively, previous ^{129}Xe MR studies mainly focused on the investigation of the effects of aging, smoking, or COPD on lung structure and function individually, whereas a comprehensive comparative evaluation of these risk factors provides enhanced diagnostic potential of COPD in the elderly population. We hypothesize that pulmonary structural and functional changes mensurated by ^{129}Xe measurements and due to aging, smoking, and lung diseases are various and worsen progressively when these factors accumulate. In this study, we comprehensively assessed the influence of aging, cigarette smoking, and COPD on pulmonary physiological parameters measured with ^{129}Xe MR and pulmonary function tests (PFTs). Airflow, ventilation maps, pulmonary morphological parameters, and gas-transfer function were evaluated for healthy young (HY) and elder volunteers, asymptomatic smokers, and subjects with COPD. Pathological changes and MR features characteristic to different risk factors were identified.

Materials and methods

Subject recruitment

This study was performed under the approval of the Institutional Review Board. Written informed consent

was obtained from each subject prior to research initiation. Self-reported smoking and lung disease history were recorded. In this exploratory prospective study, a total number of 133 subjects were recruited and the grouping and exclusion criteria were shown in Fig. 1. Subjects were divided into four groups according to age [25], smoking history, and pathology: HY group, who were younger than 44 years of age and had no history of smoking or lung diseases; age-matched control (AMC) subjects, who were older than 45 years of age and had no history of smoking or lung diseases; asymptomatic smokers (AS), who were older than 45 years of age and had no history of lung diseases with $FEV_1/FVC \geq 0.7$; COPD patients, who were older than 45 years of age with $FEV_1/FVC < 0.7$. Subjects with low SNR data ($n = 16$), repeated examinations ($n = 2$), or other lung diseases ($n = 20$) were excluded. Additionally, five young asymptomatic smokers were excluded from further analysis due to a significant age and pack-years difference compared to elderly asymptomatic smokers. The comparisons of young asymptomatic smokers with the HY and AS groups are summarized in the Supplementary Material. Ninety subjects were included in the final analysis. Prior to ^{129}Xe MR examinations, PFTs were performed for each subject using a hand-held spirometer (sp-1, Schiller AG) to obtain forced expiratory volume in the first second (FEV_1) and forced vital capacity (FVC).

Hyperpolarized xenon preparation and delivery

HP ^{129}Xe gas was generated with spin-exchange optical pumping (SEOP) [26] using a home-built polarizer. HP xenon gas was cryogenically accumulated and then thawed into a Tedlar bag [27]. Isotopically enriched xenon gas (86% ^{129}Xe) was used, and the available spin polarization of ^{129}Xe in the Tedlar bag was approximately 20%. Before HP ^{129}Xe MRI examinations, each subject was instructed to inhale 1 L of gas mixture (5% xenon and 95% N_2 by volume) from two Tedlar bags connected by a Y-shape tube from functional residual capacity (FRC) for flip angle calibration [22]. Subsequently, the subject was instructed to inhale 1 L of gas mixture (45% xenon and 55% N_2 by volume) from FRC and hold the breath for ^{129}Xe MR examinations. A total of four doses of HP xenon gas were administered to each subject.

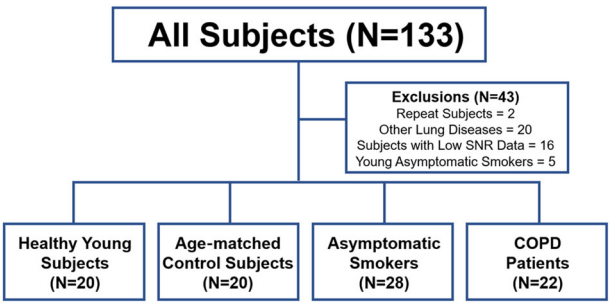

Fig. 1 The flow chart of subject recruitment. Ninety of all the 133 enrolled subjects completed the examinations and were divided into four groups according to age, smoking history, and pathology

^{129}Xe MR examinations

^{129}Xe MR acquisitions of ventilation, microstructure, and gas-transfer function were performed on a 1.5-T MRI Scanner (Avanto, Siemens) with a horizontal magnet using a home-built transmit-receive vest RF coil (17.61 MHz for ^{129}Xe).

A 3D balanced steady-state free precession (bSSFP) sequence was used for ventilation imaging. Notable parameters include repetition time/echo time (TR/TE) = 4.2/1.9 ms, matrix size = 96 × 84, field of view = 384 × 336 mm^2, slice thickness = 8 mm, bandwidth = 38.4 kHz, number of slices = 24, flip angle (FA) = 10° and acquisition time = 8.4 s. Anatomic thoracic ^{1}H images were also acquired in the same breath-hold following ventilation imaging using a 3D FLASH sequence: TR/TE = 2.4/0.7 ms, matrix size = 96 × 84, field of view = 384 × 336 mm^2, slice thickness = 8 mm, bandwidth = 48 kHz, number of slices = 24, FA = 5° and acquisition time = 2 s.

^{129}Xe diffusion-weighted imaging (DWI) was employed to assess the lung morphology with the following parameters: TR/TE = 13.9/10.9 ms, matrix size = 64 × 64, field of view = 384 × 384 mm^2, slice thickness = 30 mm, bandwidth = 16 kHz, number of slices = 4, FA = 9° and acquisition time = 8.8 s. The parameters for bipolar diffusion-weighted gradients include ramp time $\tau = 0.3$ ms, duration time $\delta = 3.7$ ms, diffusion time $\Delta = 5$ ms, b = 0, 10, 20, 30, and 40 s/cm^2. ^{129}Xe DWI was undersampled by a factor of two for each b value, and compressed sensing was used for undersampled reconstruction [28].

Chemical shift saturation recovery (CSSR) was used to assess the gas-transfer function with the following parameters: bandwidth = 10 kHz, data points = 512, acquisition time = 5.3 s, and 21 exchange times ranging from 5 ms to 700 ms.

Data processing

Ventilation defects were segmented using a hierarchical k-means clustering method. Ventilation defect percent (VDP) was quantified by normalizing the ventilation defect volumes to the thoracic cavity provided by the inherently registered ^{1}H FLASH images, as previously described [29, 30]. The signal intensities of ventilation images were classified into five clusters ranging from signal void to hyperintense signals that were labeled in

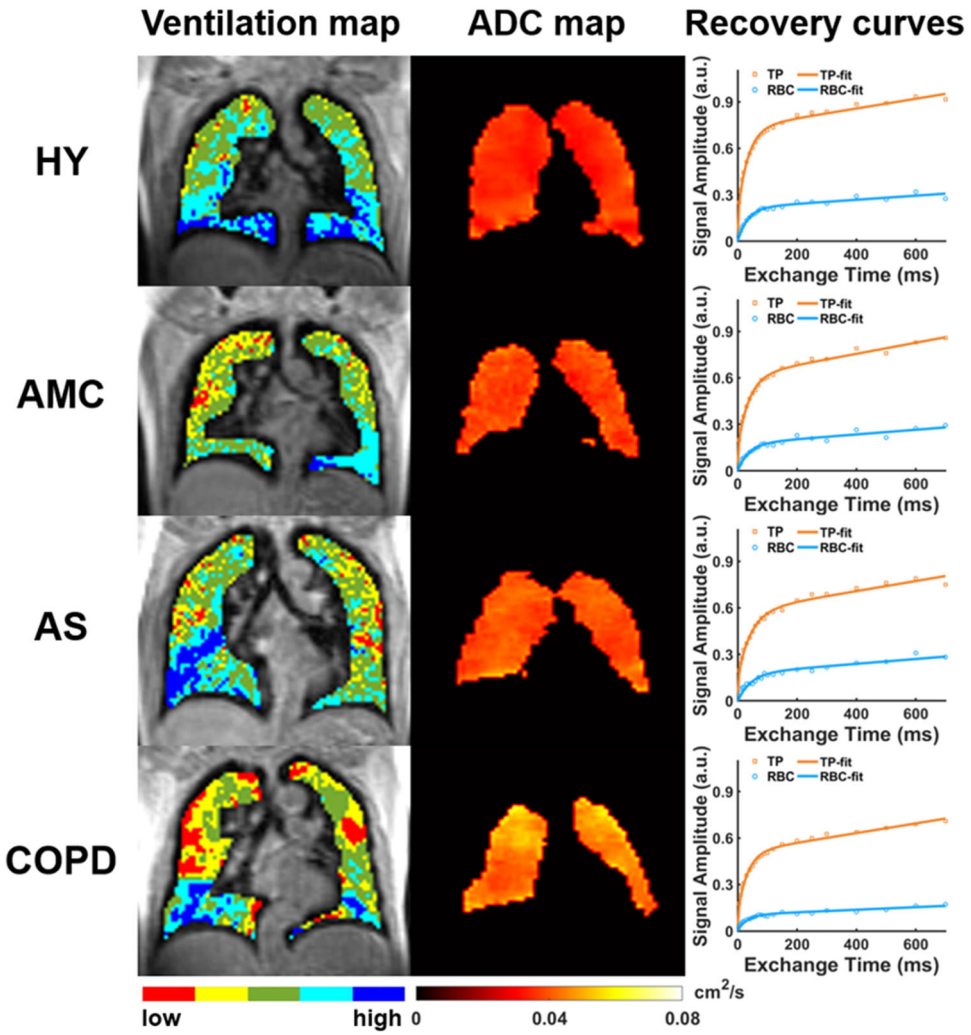

Fig. 2 The typical ventilation maps, ADC maps and dissolved xenon recovery curves from the HY (25 y.o.), AMC (59 y.o.), AS (59 y.o.) and COPD (63 y.o.) subjects, respectively. In ventilation maps, no signal (ventilation defect), hypointense, middle intense, middle high intense, and hyperintense signal were marked as red, yellow, green, aqua, and blue, respectively. ADC, apparent diffusion coefficient; a.u., arbitrary unit

red, yellow, green, aqua, and blue, as shown in Fig. 2. The DWI data was used to calculate ADC for each slice and the whole lung after segmentation and calibration of the signal attenuation from RF excitation [28]. Morphological parameters, including alveolar sleeve depth (h) and mean airspace chord length (L_m), were obtained using a cylindrical model [31]. For CSSR data, signal amplitudes of TP and RBC on each exchange time were extracted. Gas-transfer parameters, including total septal wall thickness (d), barrier thickness (δ), and hematocrit (Hct) were obtained by fitting the TP and RBC signals to the model of Xenon exchange (MOXE) using a nonlinear least squares method [32]. The ratio of xenon signal from red blood cells and interstitial tissue/plasma (RBC/TP) at the exchange time of 250 ms was also calculated [33, 34].

Statistical analysis

Data was tested for normality using the Kolmogorov–Smirnova normality test before further analysis. The parameters derived from PFTs and ^{129}Xe MRI/MRS were compared using two-tailed t-tests or Wilcoxon rank-sum tests when appropriate. The correlation between the parameters measured by ^{129}Xe MRI/MRS and age was evaluated using Spearman correlation coefficients (ρ). Age dependence with PFTs and MR characteristics was determined by univariate linear regression. $p < 0.05$ was considered statistically significant.

Results

Demographics and PFTs measurements

Ninety subjects, including 20 healthy young subjects (33.3 ± 7.5 y.o.), 20 age-matched control subjects

(60.1 ± 11.0 y.o.), 28 asymptomatic smokers (58.1 ± 7.7 y.o.), and 22 COPD patients (61.7 ± 10.4 y.o.), were included for final analysis. The subjects from the AS and COPD groups have a mean smoking history of 34.3 pack-years (13–92 pack-years) and 42.1 pack-years (20–120 pack-years), respectively. No significant differences were observed in age between the groups of AMC and AS ($p = 0.492$), AS and COPD ($p = 0.159$), and AMC and COPD ($p = 0.614$). The measured FEV_1/FVC was ≥ 0.7 for all the subjects in the HY, AMC and AS groups, and < 0.7 for the COPD group. FEV_1/FVC were 0.82 ± 0.09, 0.80 ± 0.05, 0.77 ± 0.07, and 0.59 ± 0.14 for the HY, AMC, AS, and COPD groups, respectively. There were significant differences in FEV_1/FVC between the groups of AS and COPD ($p < 0.001$) and the groups of AMC and COPD ($p < 0.001$). Table 1 shows the demographics and PFT measures for the 90 participants.

Representative ^{129}Xe MR measurements

Figure 2 shows representative ^{129}Xe ventilation images, ADC maps, and dissolved ^{129}Xe recovery curves for a healthy young subject (male, 25 years old), an age-matched subject (female, 59 years old), an asymptomatic smoking subject (male, 59 years old), and a COPD patient (male, 63 years old). As shown in Fig. 2, the ventilation defect volumes were increased for the subjects in the AMC, AS, and COPD groups compared with the HY subject. ADC maps were homogenous and comparable for the HY, AMC, and AS subjects but heterogeneous for the COPD patient.

Comparison of HY and AMC groups

The comparison of the ^{129}Xe MRI/MRS parameters between HY and AMC groups was shown in Fig. 3. The VDP values were 1.3% and 2.5% in the HY and AMC groups, respectively, indicating a significant difference ($p = 0.035$). The microstructural parameters obtained from ^{129}Xe measurements showed a significant difference in alveolar sleeve depth measurement h between the two groups ($p = 0.003$), but no significant differences were found in L_m and ADC measurements. In the gas-transfer function, a significant difference was observed in RBC/TP ratios ($p = 0.002$), which were 0.42 ± 0.11 for the young group and 0.30 ± 0.08 for the AMC group. However, no significant difference was detected in total septal wall thickness d ($p = 0.790$). These results were summarized in Table 1.

The relationships between age and ^{129}Xe MR measurements are depicted in Fig. 4 for all the subjects in the HY and AMC groups. The measured h, HCT, and RBC/TP were negatively correlated with age with $\rho = -0.65$ ($p < 0.001$), -0.71 ($p < 0.001$), and -0.76 ($p < 0.001$), respectively. There were positive correlations between age and VDP ($\rho = 0.49$, $p = 0.013$) and δ ($\rho = 0.59$, $p < 0.001$). However, there were no significant correlations between age and L_m ($\rho = 0.21$, $p = 0.195$), ADC ($\rho = 0.25$, $\rho = 0.125$), and d ($\rho = 0.14$, $p = 0.444$).

Table 1 The demographics, PFTs and HP ^{129}Xe MR results for all the subjects

Parameter	Mean ± standard deviation				Significant differences (*p* value)			
	HY ($n = 20$)	AMC ($n = 20$)	AS ($n = 28$)	COPD ($n = 22$)	HY-AMC	AMC-AS	AMC-COPD	AS-COPD
Demographics								
Sex	10 M/10 F	4 M/16 F	25 M/3 F	15 M/7 F	/	/	/	/
Smoking (pack years)	0	0	34.3 ± 18.4	42.1 ± 22.7	/	/	/	/
Age (years)	33.3 ± 7.5	60.1 ± 11.0	58.1 ± 7.7	61.7 ± 10.4	< 0.001	0.492	0.614	0.159
Pulmonary function tests								
FEV_1/FVC	0.82 ± 0.09	0.80 ± 0.05	0.77 ± 0.07	0.59 ± 0.14	0.569	0.066	< 0.001	< 0.001
Ventilation								
VDP (%)	1.3 ± 1.0	2.5 ± 1.4	4.3 ± 1.7	11.4 ± 7.2	0.035	0.020	< 0.001	0.003
Lung morphometry parameters								
h (μm)	194 ± 8	181 ± 17	183 ± 12	156 ± 22	0.003	0.896	< 0.001	< 0.001
L_m (μm)	211 ± 21	220 ± 25	233 ± 30	355 ± 85	0.369	0.144	< 0.001	< 0.001
ADC (cm^2/s)	0.034 ± 0.003	0.035 ± 0.003	0.036 ± 0.004	0.048 ± 0.008	0.299	0.175	< 0.001	< 0.001
Gas-transfer function								
d (μm)	9.9 ± 0.7	10.0 ± 0.9	10.9 ± 1.8	12.1 ± 0.7	0.790	0.048	< 0.001	0.008
δ (μm)	1.0 ± 0.3	1.4 ± 0.3	1.4 ± 0.5	1.5 ± 0.4	0.002	0.911	0.259	0.257
Hct	0.22 ± 0.04	0.17 ± 0.04	0.16 ± 0.04	0.14 ± 0.03	0.002	0.309	0.011	0.113
RBC/TP	0.43 ± 0.11	0.31 ± 0.08	0.27 ± 0.07	0.23 ± 0.05	0.002	0.116	0.001	0.035

M male, *F* female, *h* alveolar sleeve depth, L_m, mean airspace chord length, *d* total septal wall thickness, *δ* barrier thickness, *Hct* blood hematocrit

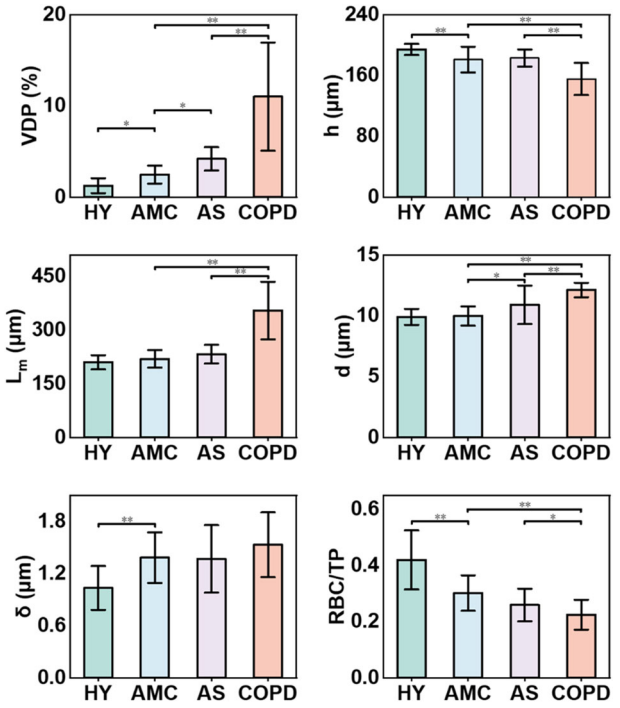

Fig. 3 Physiological parameters of the four groups measured with ^{129}Xe MRI/MRS. The bar graphs displayed the average and standard deviation of these physiological parameter values. Asterisks indicate significant differences between two cohorts as determined by two-tailed t-tests or Wilcoxon rank-sum tests. * $p < 0.05$, ** $p < 0.01$. VDP, ventilation defects percent; h, alveolar sleeve depth; L_m, mean airspace chord length; d, total septal wall thickness; δ, barrier thickness; RBC/TP, the ratio of xenon signal from red blood cells and interstitial tissue/plasma. Due to significant age disparities, the comparisons between the HY and AS groups, as well as between the HY and COPD groups, were not presented

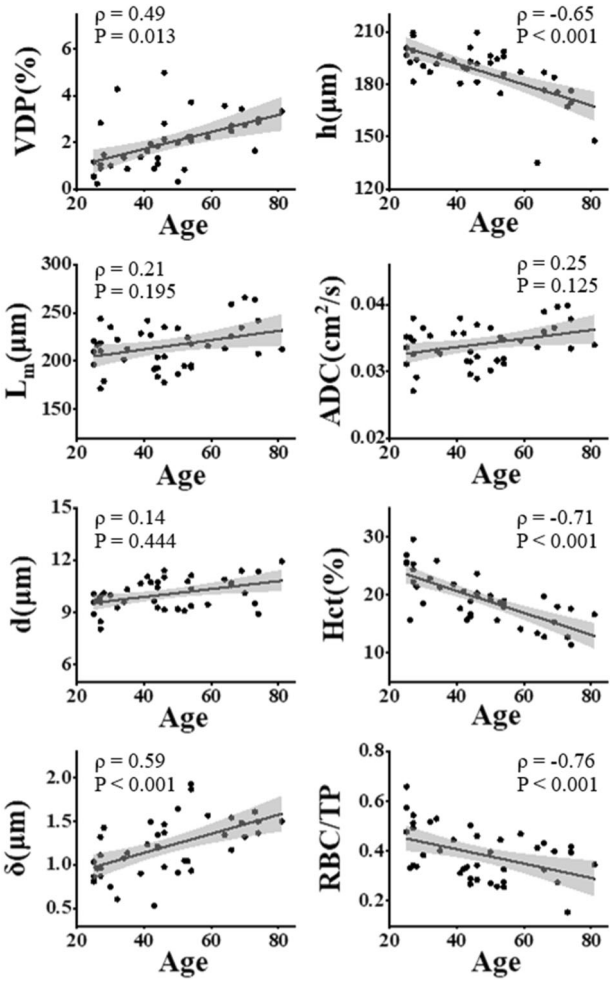

Fig. 4 The correlation between the age and the physiological parameters measured with ^{129}Xe MR in the healthy group (HY and AMC groups). Significant correlations were found between the age and the measured VDP, alveolar sleeve depth (h), Hct, barrier thickness (δ), and ratio of xenon signal from RBC/TP. The lines represent univariate linear fits with 95% confidence intervals (shaded). L_m, mean airspace chord length, d total septal wall thickness

Comparison of AMC and AS groups

As depicted in Fig. 3, a significant difference ($p = 0.020$) was observed in the VDP measurements between the AMC and AS groups, with values were 2.5% and 4.3%, respectively. No substantial differences were identified in the microstructural parameters provided by ^{129}Xe measurements across the groups ($p = 0.144$ for L_m, $p = 0.896$ for h, and $p = 0.175$ for ADC). In terms of the gas-transfer function, a significant difference was noted in the total septal wall thickness (d) between the AMC and AS groups ($p = 0.048$). Meanwhile, no significant differences were observed in RBC/TP ratios ($p = 0.116$), barrier thickness δ ($p = 0.911$), and blood hematocrit Hct ($p = 0.309$).

Comparison of AMC and COPD groups

The measured VDP values were 2.5% and 11.4% for the AMC and COPD groups, respectively, demonstrating a significant difference ($p < 0.001$). In comparison to the AMC group, the COPD group exhibited higher L_m and ADC measurements, with significant differences ($p < 0.001$ for both L_m and ADC), while the h measurement was lower, also showing a significant difference ($p < 0.001$). The gas-transfer function revealed RBC/TP ratios of 0.30 ± 0.08 and 0.22 ± 0.06 for the AMC and COPD groups, respectively, indicating a significant difference ($p = 0.001$). Additionally, a notable difference was observed in the total septal wall thickness (d) between the groups. These results were summarized in Table 1.

Comparison of AS and COPD groups

A significant difference ($p = 0.003$) was identified between the AS and COPD groups in terms of VDP measurement, with values of 4.3% and 11.4%, respectively. Furthermore, significant differences were

observed in L_m, h, and ADC measurements between the two groups ($p < 0.001$ for L_m, $p < 0.001$ for h, and $p < 0.001$ for ADC). The ADC map for the COPD subjects displayed visible heterogeneity across the lung, indicating enlarged airspaces. In relation to the gas-transfer function, the RBC/TP ratios were found to be 0.27 ± 0.07 in the AS group and 0.23 ± 0.05 in the COPD group, presenting a significant difference ($p = 0.035$). Additionally, there was a significant difference in total septal wall thickness d between the two groups ($p = 0.008$). These results were summarized in Table 1.

Radar plots of FEV_1/FVC and ^{129}Xe MR features for different groups

Figure 5 shows the radar plots of FEV_1/FVC and ^{129}Xe MRI/MRS features for different groups to characterize the influences of aging, smoking, and COPD. For the AMC group, the main discrepancies were VDP and RBC/TP compared with the HY group. Compared with the AMC group, only VDP and d were predominantly different for the AS subjects. Compared with the AS group, all the parameters were statistically and significantly different for the COPD patients.

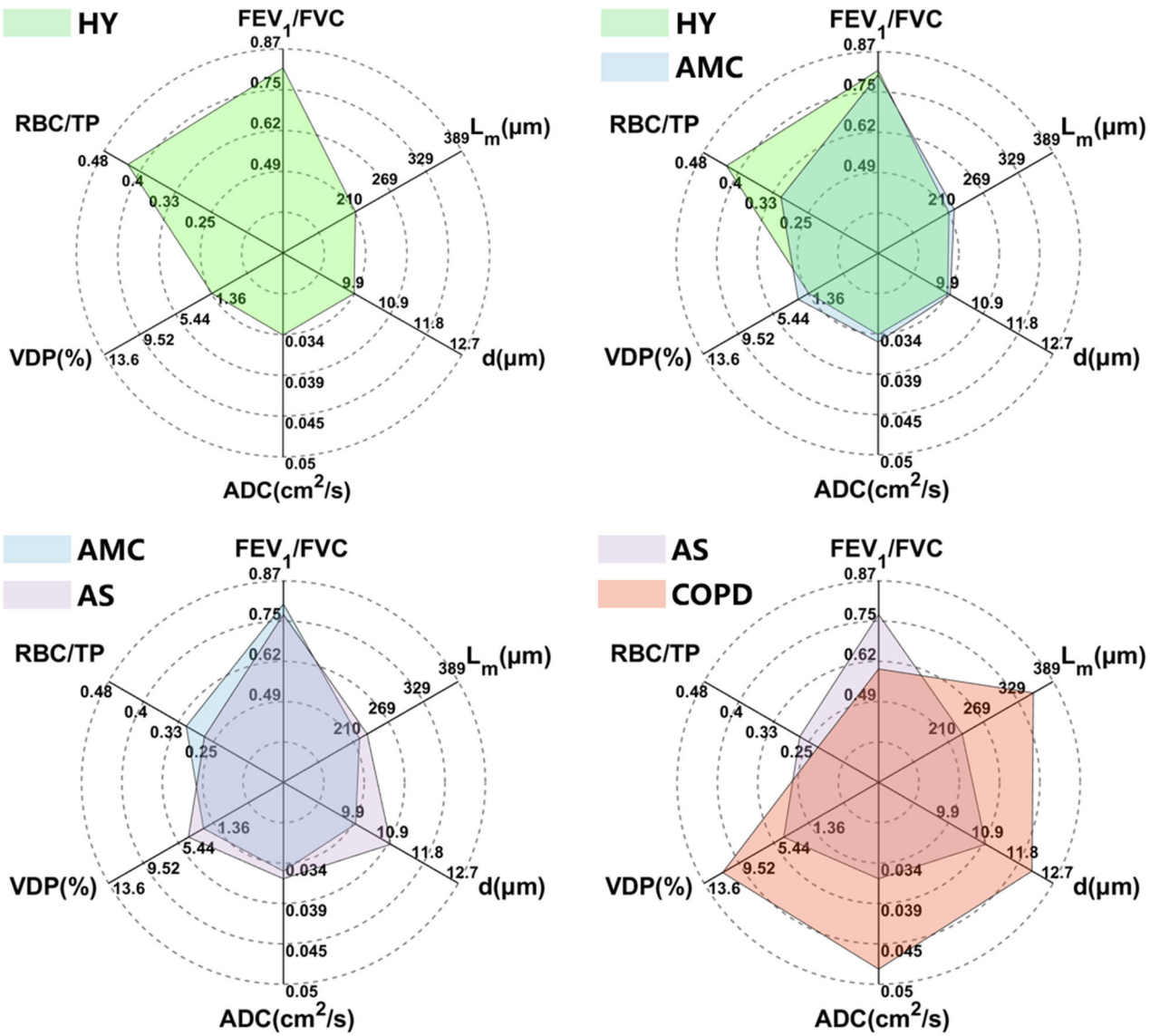

Fig. 5 Radar plots to display the primary PFTs and ^{129}Xe MR signatures associated with different groups. The mean values of the markers in each group are plotted on one of the six radial directions, including FEV_1/FVC, VDP, ADC, mean airspace chord length (L_m), total septal wall thickness (d), and ratio of xenon signal from RBC/TP

Discussion

In this study, we employed hyperpolarized ^{129}Xe MR to comprehensively assess the pulmonary physiological changes caused by aging, cigarette smoking, and COPD. PFTs and ^{129}Xe MR ventilation, microstructure, and gas-transfer function were measured and compared for 90 subjects with different pulmonary pathologies. Results indicate that pulmonary physiological changes caused by different risk factors are various and worsen progressively when these risk factors are accumulated. These findings might be helpful for identifying pulmonary injuries caused by various factors.

The ^{129}Xe MR measurements showed that aging is a significant factor contributing to physiological changes in the lung, even for elderly subjects with normal FEV_1/FVC. Compared with the HY volunteers, the AMC subjects had significantly higher VDP and lower RBC/TP consistent with previous studies [35, 36]. Compared with the HY group, the reduced alveolar sleeve depth (h) in the AMC group may be explained by the age-related pulmonary structure remodeling processes [23]. Moreover, we also found significant differences between the HY and AMC groups in the gas-transfer functional parameters (δ and Hct). Although ADC and L_m are increased with age due to the enlargement of alveoli during the human ontogeny [37], no significant differences were observed between the HY and AMC groups in this study. This might be attributed to the fundamental structure of alveoli that typically remains relatively stable once adulthood is reached [38, 39]. Our results suggest that h was more sensitive to aging than L_m and ADC.

Cigarette smoking represents a major contributor to cellular damage and subsequent pulmonary structural and functional impairment. Significant differences in gas-transfer function were observed between the AS and AMC groups. Although the morphometric parameters were comparable between these two groups, VDP was greater with statistical significance for the AS group. This might be attributed to smoking-induced lung damage, including airway inflammation and emphysema, as previously reported [40]. In addition, we observed higher d in the AS group, which might be caused by the swelling of the septal walls in the processes of inflammatory or permanent remodeling that involves the synthesis of additional connective tissues [12].

Compared with the AS group, subjects in the COPD group exhibited more severe physiological injuries. Apart from the previously reported lower FEV_1/FVC, higher ADC and d values [12], we found significantly higher VDP and L_m and lower h in the COPD group versus the AS group. In addition, the COPD patients tended to have a higher d and lower RBC/TP relative to the AS subjects, probably due to the exacerbation of inflammatory processes [22].

Previous studies investigated individual risk factors, such as age, smoking, or COPD, utilizing subset measurements of ventilation, microstructure, and gas-transfer function [12, 35, 41]. However, the impact of these risk factors on various physiological parameters derived from all three measurements within the same cohort remains unknown. In contrast to previous studies, we simultaneously investigated the cumulative effects of aging, cigarette smoking, and COPD on lung function, utilizing a series of comprehensive experiments including ventilation, microstructure, and gas-transfer function. Consequently, we were able to simultaneously and thoroughly evaluate the physiological alterations associated with risk factors impacting ventilation, microstructure, and gas-transfer function within identical cohorts. For example, our findings revealed that VDP, h, Hct, and RBC/TP derived from ^{129}Xe MR measurements exhibited sensitivity to both age and COPD. However, L_m, ADC, and d demonstrated sensitivity solely to the factor of COPD, which could provide more information when considering the aging effect to COPD progression. Additionally, we evaluated the influence of these risk factors when accumulated using radar plots, and observe increased d in the AS group compared with the AMC group with further increase in the COPD group. Our study comprehensively investigated various lung physiological effects induced by age, smoking, and COPD, and compare the discrepancies of lung ventilation, microstructure, and gas-transfer function induced by different risk factors in a single integrated investigation, which was previously not available.

Our study was limited in several ways. First, carbon monoxide diffusion capacity (DL_{CO}), an important clinical indicator of pulmonary diffusing capacity, was not included in this study for the limited function of spirometry. As an exploratory study, we used a relatively small dataset of 90 subjects with a limited diversity of lung conditions. Gender matching and sample size calculation were also not specifically considered in this study, as they have been done in previous studies [23, 42–44]. A larger gender-matched population with diverse lung pathologies will be considered to minimize the biases in further studies. In addition, here we employed ^{129}Xe MRS analysis to evaluate the gas-transfer abnormalities globally and gas-transfer imaging may be included for regional and potentially more sensitive assessment of lung injury. These limitations represent our research directions in the future.

Conclusions

In this study, the influences of aging, cigarette smoking, and disease (COPD) on the changes of pulmonary physiology were comprehensively assessed using ^{129}Xe MR. The measured pulmonary structural and functional

changes caused by different risk factors vary substantially and worsen progressively when these factors are accumulated. These results may help in identifying the underlying causes of lung physiological changes and diagnosing COPD at different age stages.

Abbreviations

ADC	Apparent diffusion coefficient
AMC	Age-matched control
AS	Asymptomatic smokers
COPD	Chronic obstructive pulmonary disease
CSSR	Chemical shift saturation recovery
CT	Computed tomography
d	Total septal wall thickness
DWI	Diffusion-weighted imaging
FEV_1	Forced expiratory volume in the first second
FRC	Functional residual capacity
FVC	Forced vital capacity
h	Alveolar sleeve depth
Hct	Blood hematocrit
HP	Hyperpolarized
HY	Healthy young
L_m	Mean airspace chord length
PFTs	Pulmonary function tests
RBC	Red blood cell
RBC/TP	Ratio of xenon signal from red blood cells and interstitial tissue/plasma
TP	Tissue/plasma
VDP	Ventilation defects percent
δ	Barrier thickness

Supplementary information

The online version contains supplementary material available at https://doi.org/10.1007/s00330-024-10800-w.

Funding

This work is supported by National key Research and Development Program of China (grant no. 2018YFA0704000, 2022YFC2410000), National Natural Science Foundation of China (grant no. 82127802, 21921004, 82372150, 81930049, 82202119), the Strategic Priority Research Program of the Chinese Academy of Sciences (grant No. XDB0540000), Key Research Program of Frontier Sciences, CAS (grant no. ZDBS-LY-JSC004), Hubei Provincial Key Technology Foundation of China(2021ACA013, 2023BAA021) and Hubei Provincial Outstanding Youth Fund (2023AFA112). Haidong Li and Xiuchao Zhao acknowledge the support from Youth Innovation Promotion Association, CAS (grant no. 2020330, 2021330).

Compliance with ethical standards

Guarantor

The scientific guarantor of this publication is Xin Zhou.

Conflict of interest

The authors of this manuscript declare no relationships with any companies whose products or services may be related to the subject matter of the article.

Statistics and biometry

No complex statistical methods were necessary for this paper.

Informed consent

Written informed consent was obtained from all subjects (patients) in this study.

Ethical approval

This study was performed under the approval of the Institutional Review Board at Innovation Academy for Precision Measurement Science and Technology, Chinese Academy of Sciences. Ethical code: APMH22005A.

Study subjects or cohorts overlap

Study subjects have not been previously reported or published before.

Methodology

- Prospective
- Experimental
- Performed at one institution

Author details

[1]Key Laboratory of Magnetic Resonance in Biological Systems, State Key Laboratory of Magnetic Resonance and Atomic and Molecular Physics, National Center for Magnetic Resonance in Wuhan, Wuhan Institute of Physics and Mathematics, Innovation Academy for Precision Measurement Science and Technology, Chinese Academy of Sciences–Wuhan National Laboratory for Optoelectronics, Huazhong University of Science and Technology, Wuhan 430071, China. [2]University of Chinese Academy of Sciences, Beijing 100049, China. [3]Department of Radiology, Changzheng Hospital of the Second Military Medical University, Shanghai 200003, China. [4]School of Biomedical Engineering, Hainan University, Haikou 570228, China.

Received: 14 March 2024 Revised: 14 March 2024 Accepted: 5 April 2024
Published online: 15 May 2024

References

1. Safiri S, Carson-Chahhoud K, Noori M et al (2022) Burden of chronic obstructive pulmonary disease and its attributable risk factors in 204 countries and territories, 1990-2019: results from the Global Burden of Disease Study 2019. BMJ 378:e069679
2. Feenstra TL, van Genugten ML, Hoogenveen RT, Wouters EF, Rutten-van Molken MP (2001) The impact of aging and smoking on the future burden of chronic obstructive pulmonary disease: a model analysis in the Netherlands. Am J Respir Crit Care Med 164:590–596
3. MacNee W (2016) Is Chronic Obstructive Pulmonary Disease an accelerated aging disease? Ann Am Thorac Soc 13:S429–S437
4. Tuder RM (2006) Aging and cigarette smoke: fueling the fire. Am J Respir Crit Care Med 174:490–491
5. Poels PJ, Schermer TR, van Weel C, Calverley PM (2006) Spirometry in chronic obstructive pulmonary disease. BMJ 333:870–871
6. Bhatt NY, Wood KL (2008) What defines abnormal lung function in older adults with chronic obstructive pulmonary disease? Drugs Aging 25:717–728
7. Park J, Hobbs BD, Crapo JD et al (2020) Subtyping COPD by using visual and quantitative CT imaging features. Chest 157:47–60
8. Doganay O, Kim M, Gleeson FV (2023) Gas exchange and ventilation imaging of healthy and COPD subjects using hyperpolarized xenon-129 MRI and a 3D alveolar gas-exchange model. Eur Radiol 33:3322–3331
9. Niedbalski PJ, Hall CS, Castro M et al (2021) Protocols for multi-site trials using hyperpolarized Xe-129 MRI for imaging of ventilation, alveolar-airspace size, and gas exchange: a position paper from the Xe-129 MRI clinical trials consortium. Magn Reson Med 86:2966–2986
10. Virgincar RS, Cleveland ZI, Kaushik SS et al (2013) Quantitative analysis of hyperpolarized 129Xe ventilation imaging in healthy volunteers and subjects with chronic obstructive pulmonary disease. NMR Biomed 26:424–435
11. Ouriadov A, Farag A, Kirby M, McCormack DG, Parraga G, Santyr GE (2013) Lung morphometry using hyperpolarized (129) Xe apparent diffusion coefficient anisotropy in chronic obstructive pulmonary disease. Magn Reson Med 70:1699–1706
12. Ruppert K, Qing K, Patrie JT, Altes TA, Mugler 3rd JP (2019) Using hyperpolarized Xenon-129 MRI to quantify early-stage lung disease in smokers. Acad Radiol 26:355–366

13. Kirby M, Ouriadov A, Svenningsen S et al (2014) Hyperpolarized 3He and 129Xe magnetic resonance imaging apparent diffusion coefficients: physiological relevance in older never- and ex-smokers. Physiol Rep 2:e12068
14. He M, Driehuys B, Que LG, Huang YT (2016) Using hyperpolarized (129)Xe MRI to quantify the pulmonary ventilation distribution. Acad Radiol 23:1521–1531
15. Sheikh K, Paulin GA, Svenningsen S et al (2014) Pulmonary ventilation defects in older never-smokers. J Appl Physiol (1985) 117:297–306
16. Woodhouse N, Wild JM, Paley MN et al (2005) Combined helium-3/proton magnetic resonance imaging measurement of ventilated lung volumes in smokers compared to never-smokers. J Magn Reson Imaging 21:365–369
17. Fain SB, Panth SR, Evans MD et al (2006) Early emphysematous changes in asymptomatic smokers: detection with 3He MR imaging. Radiology 239:875–883
18. Polverino F, Hysinger EB, Gupta N et al (2020) Lung MRI as a potential complementary diagnostic tool for early COPD. Am J Med 133:757–760
19. Thomen RP, Quirk JD, Roach D et al (2017) Direct comparison of (129) Xe diffusion measurements with quantitative histology in human lungs. Magn Reson Med 77:265–272
20. Xie J, Li H, Zhang H et al (2019) Single breath-hold measurement of pulmonary gas exchange and diffusion in humans with hyperpolarized (129) Xe MR. NMR Biomed 32:e4068
21. Wang Z, He M, Bier E et al (2018) Hyperpolarized (129) Xe gas transfer MRI: the transition from 1.5T to 3T. Magn Reson Med 80:2374–2383
22. Qing K, Mugler 3rd JP, Altes TA et al (2014) Assessment of lung function in asthma and COPD using hyperpolarized 129Xe chemical shift saturation recovery spectroscopy and dissolved-phase MRI. NMR Biomed 27:1490–1501
23. Quirk JD, Sukstanskii AL, Woods JC et al (2016) Experimental evidence of age-related adaptive changes in human acinar airways. J Appl Physiol (1985) 120:159–165
24. Willmering MM, Walkup LL, Niedbalski PJ et al (2022) Pediatric (129) Xe gas-transfer MRI-feasibility and applicability. J Magn Reson Imaging 56:1207–1219
25. Ahmad OB, Boschi-Pinto C, Lopez AD, Murray CJ, Lozano R, Inoue M, Age standardization of rates: a new WHO standard, 2001. http://www.who.int/healthinfo/paper31.pdf
26. Zhou X, Luo J, Sun X et al (2004) Enhancement of solid-state proton NMR via the spin-polarization-induced nuclear Overhauser effect with laser-polarized xenon. Phys Rev B 70:052405
27. Li H, Zhang Z, Zhao X, Sun X, Ye C, Zhou X (2016) Quantitative evaluation of radiation-induced lung injury with hyperpolarized xenon magnetic resonance. Magn Reson Med 76:408–416
28. Zhang H, Xie J, Xiao S et al (2018) Lung morphometry using hyperpolarized (129) Xe multi-b diffusion MRI with compressed sensing in healthy subjects and patients with COPD. Med Phys 45:3097–3108
29. Kirby M, Heydarian M, Svenningsen S et al (2012) Hyperpolarized 3He magnetic resonance functional imaging semiautomated segmentation. Acad Radiol 19:141–152
30. Li H, Zhao X, Wang Y et al (2021) Damaged lung gas exchange function of discharged COVID-19 patients detected by hyperpolarized 129Xe MRI. Sci Adv 7:eabc8180
31. Yablonskiy DA, Sukstanskii AL, Quirk JD, Woods JC, Conradi MS (2014) Probing lung microstructure with hyperpolarized noble gas diffusion MRI: theoretical models and experimental results. Magn Reson Med 71:486–505
32. Chang YV, Quirk JD, Ruset IC, Atkinson JJ, Hersman FW, Woods JC (2014) Quantification of human lung structure and physiology using hyperpolarized 129Xe. Magn Reson Med 71:339–344
33. Ruppert K, Amzajerdian F, Hamedani H et al (2019) Assessment of flip angle-TR equivalence for standardized dissolved-phase imaging of the lung with hyperpolarized 129Xe MRI. Magn Reson Med 81:1784–1794
34. Niedbalski PJ, Lu J, Hall CS et al (2022) Utilizing flip angle/TR equivalence to reduce breath hold duration in hyperpolarized (129) Xe 1-point Dixon gas exchange imaging. Magn Reson Med 87:1490–1499
35. Plummer JW, Willmering MM, Cleveland ZI, Towe C, Woods JC, Walkup LL (2023) Childhood to adulthood: accounting for age dependence in healthy-reference distributions in (129) Xe gas-exchange MRI. Magn Reson Med 89:1117–1133
36. Mummy D, Swaminathan A, Yarnall K et al (2022) Hyperpolarized ^{129}Xe MRI in healthy control subjects reveals age-related changes in measurements of ventilation and red blood cell transfer. Am J Respir Crit Care Med 205:A2548
37. Aghasafari P, Heise RL, Reynolds A, Pidaparti RM (2019) Aging effects on alveolar sacs under mechanical ventilation. J Gerontol A Biol Sci Med Sci 74:139–146
38. Hsia CC, Hyde DM, Weibel ER (2016) Lung structure and the intrinsic challenges of gas exchange. Compr Physiol 6:827–895
39. Bowdish DME (2019) The aging lung: is lung health good health for older adults? Chest 155:391–400
40. Pike D, Kirby M, Guo F, McCormack DG, Parraga G (2015) Ventilation heterogeneity in ex-smokers without airflow limitation. Acad Radiol 22:1068–1078
41. Stewart NJ, Horn FC, Norquay G et al (2017) Reproducibility of quantitative indices of lung function and microstructure from (129) Xe chemical shift saturation recovery (CSSR) MR spectroscopy. Magn Reson Med 77:2107–2113
42. Mummy DG, Bier EA, Wang ZY et al (2021) Hyperpolarized Xe-129 MRI and spectroscopy of gas-exchange abnormalities in nonspecific interstitial pneumonia. Radiology 301:211–220
43. Wang Z, Bier EA, Swaminathan A et al (2019) Diverse cardiopulmonary diseases are associated with distinct xenon magnetic resonance imaging signatures. Eur Respir J 54:1900831
44. Chan HF, Collier GJ, Weatherley ND, Wild JM (2019) Comparison of in vivo lung morphometry models from 3D multiple b-value (3) He and (129) Xe diffusion-weighted MRI. Magn Reson Med 81:2959–2971

Publisher's Note